Local susceptibilities in the paramagnetic regime of $Y(Fe,Al)_2$

1993 J. Phys.: Condens. Matter 5 7277

(http://iopscience.iop.org/0953-8984/5/39/015)

J. Phys.: Condens. Matter 5 (1993) 7277–7288. Printed in the UK

Local susceptibilities in the paramagnetic regime of $Y(Fe,Al)_2$

A Pösinger†, M Reissner†, W Steiner†, P Blaha‡, P Mohn‡ and K Schwarz‡

† Institut für Angewandte und Technische Physik, Technische Universität Wien, Austria
‡ Institut für Technische Elektrochemie, Technische Universität Wien, Austria

Received 29 March 1993, in final form 23 June 1993

Abstract. The local susceptibilities of $Y(Fe,Al)_2$ are determined by high-field ^{57}Fe Mössbauer measurements and are compared with the results of ASW and LAPW band-structure calculations. The effective field acting on the ^{57}Fe nuclei arises not only from the applied field but also from core and valence contributions, with opposite signs. With decreasing Fe concentration the valence contribution increases and reaches a magnitude comparable with the core contribution which remains nearly constant. The local susceptibility stays about the same when Fe is surrounded mainly by Al but increases for more than three nearest Fe neighbours, indicating that Fe carries a magnetic moment even when it is completely surrounded by Al. The Mössbauer results are in excellent agreement with the effective Fe moments derived from bulk magnetization measurements.

1. Introduction

The magnetic behaviour of iron in the cubic Laves phases $Y(Fe_xAl_{1-x})_2$ has attracted much interest in the last two decades (see, e.g., [1–12]). YAl_2 is a Pauli paramagnet with a nearly temperature-independent susceptibility of 0.8×10^{-6} emu g^{-1} at room temperature, whereas YFe_2 has long-range order, which for a long time was interpreted to be ferromagnetic, where only the iron atoms carry a moment of about $1.45\mu_B$. However, band-structure calculations [13, 14] have shown that yttrium carries a small (compared with Fe), strongly delocalized moment, which is antiparallel to the (spatially) more localized iron moment. Subsequently this prediction was verified by diffraction measurements using polarized neutrons [15], where a moment of $(1.77 \pm 0.08)\mu_B$ for iron and a moment of $-(0.67 \pm 0.04)\mu_B$ for yttrium was determined. 80% of this yttrium moment results from spin and 20% from orbital contributions.

With increasing substitution of iron by aluminium the long-range order diminishes rapidly. Below 78 at.% Fe, only short-range order is present; this is called a mictomagnet or cluster glass [16]. In this region the samples consist of small magnetic clusters (three to ten atoms) which are nearly uncoupled and, below the so-called freezing temperature T_f, history effects appear. At higher temperatures, short-range order still exists, which is responsible for the non-linear field dependence of the magnetization. Only for temperatures higher than about $7T_f$ is pure paramagnetic behaviour found [11].

At about 80 at.% Fe, very complex magnetic behaviour is observed with both a Curie temperature (determined from Arrott plots) and a history effect at low temperatures.

On the Fe-rich side the susceptibility χ determined from bulk magnetic measurements exhibits Curie–Weiss behaviour, whereas on the Al-rich side this Curie–Weiss term has a Pauli-type matrix contribution χ_0 superimposed. χ_0 increases with increasing Fe content, indicating an enhancement of the polarization of the matrix [5].

0953-8984/93/397277+12$07.50

Under the early assumption (which is justified under certain conditions and will be discussed in section 4) that only iron carries a magnetic moment, susceptibility measurements up to 1000 K yield an effective moment $\mu_{\text{eff}} = g\mu_B\sqrt{S(S+1)}$, which only mildly depends on x. It decreases from about $3\mu_B$ per Fe atom for YFe_2 to slightly below $2\mu_B$ per Fe atom for $Y(Fe_{0.1}Al_{0.9})_2$ [5]. This points to a non-vanishing Fe moment that stays relatively constant over the entire concentration range. However, the ^{57}Fe Mössbauer investigations indicate that the electrostatic and magnetic hyperfine interactions are strongly affected by the iron environment [6]. Thus the question arises whether or not the iron moment itself depends on the local coordination.

^{57}Fe Mössbauer measurements in applied fields give one the opportunity to study the changes in local susceptibilities and moments, as has been demonstrated for example for iron diluted in a variety of different alloys (see, e.g., [17–21]).

Band-structure calculations on $Y(Fe,Al)_2$ have shown a reduction in the density of states (DOS) for low iron contents [22, 23], but they were non-spin-polarized calculations, so that a conclusive statement concerning the stability of the moment cannot be made. Another case with controversial results concerning the iron moment is the system iron in aluminium; indications for a non-magnetic Fe atom are found from experiment [24, 25], whereas first-principle calculations [26, 27] predicts a value of $1.7\mu_B$ per Fe atom. Guenzburger and Ellis [28] have shown that for these alloys the existence of the iron moment strongly depends on the lattice constant.

It is the purpose of this work to investigate the stability of the iron moment in the paramagnetic region of $Y(Fe,Al)_2$ by determining the local susceptibilities from high-field Mössbauer measurements and to compare the results with those obtained from spin-polarized band-structure calculations.

2. Experimental details

^{57}Fe Mössbauer experiments in high applied fields B_a were carried out on four representative samples of $Y(Fe_xAl_{1-x})_2$ with $x = 0.25$, 0.40, 0.65 and 0.75 (details of the preparation have been given in [5]) of thicknesses 8 mg Fe cm^{-2}, 7 mg Fe cm^{-2}, 6 mg Fe cm^{-2} and 8 mg Fe cm^{-2}, respectively. The highest measurement temperature was 300 K for all samples (because of the experimental set-up) and the lowest temperatures were 50 K, 100 K, 160 K and 280 K, respectively. These temperatures are much higher than the corresponding T_f (about 4 K, 9.5 K, 26 K and 39 K for the four samples). Within these temperature intervals the respective magnetization versus field curves are straight lines, indicating that short-range order effects are negligible.

External fields B_a of up to 13.5 T were produced by superconducting coils and controlled with a Hall probe. The accuracy of the field was ±0.01 T, with a homogeneity of 0.1% over a cylinder with 2 mm height and 15 mm diameter. The source was situated in a field-compensated area (less than 0.1 T). The direction of the field was parallel to the γ-ray direction. An additional counter was mounted above the Mössbauer drive to allow simultaneous calibration measurements. The temperature of the absorber was measured with a carbon-glass resistor and controlled with a field-independent (±1 mK per 15 T) capacity sensor.

The spectra were analysed by solving the complete Hamiltonian with magnetic and quadrupole splitting in the fast-relaxation limit within the thin-absorber approximation [29]. The finite thickness of the absorbers was taken into account using the correction formulae of Mørup and Both [30]. The subspectra were constrained to have decreasing centre shift

and increasing quadrupole splitting with increasing Fe content in the environment. This constraint follows from the analysis of magnetically unsplit spectra taken for samples with different x. For all subspectra the value for the full width at half-height was fixed to that obtained by measurements of an α-Fe foil. The asymmetry parameter was set to zero.

3. Theory

Spin-polarized band-structure calculations were performed for YFe_2 and for ordered structures of Y_2Fe_3Al, $Y_2Fe_2Al_2$ and Y_2FeAl_3 at the experimental lattice constants (7.36 Å, 7.48 Å, 7.61 Å and 7.74 Å, respectively). The calculations are based on the local-spin-density approximation (LSDA) using both the augmented spherical wave (ASW) [31] and the full potential linearized augmented plane-wave (LAPW) method [32]. The results obtained by the latter method for isomer shifts and electric field gradients have already been published [33]. In the ASW method the wavefunctions are treated non-relativistically, while in the LAPW method a fully relativistic treatment of the core states and a scalar-relativistic treatment of the valence states was used. In the calculation of the hyperfine fields, only the Fermi contact term is included, neglecting the magnetic dipole and the orbital momentum term, which for iron are generally at least an order of magnitude smaller. In the non-relativistic limit the total hyperfine field B_{tot}^{th} at the Fe nucleus is obtained directly from the respective spin densities at the nucleus:

$$B_{tot}^{th} = \tfrac{8}{3}\pi\mu_B^2[\rho_\uparrow(0) - \rho_\downarrow(0)]. \tag{1}$$

In the LAPW method a procedure derived by Blügel *et al* [34] is used; they showed that in the relativistic case the spin density at the origin should be replaced by its average over the Thomson radius $r_T = Ze^2/mc^2$.

4. Results

Mössbauer spectra at room temperature without the applied field exhibit only quadrupole splitting for $0.1 \leqslant x \leqslant 0.85$. The asymmetry of these spectra depends on x and can be explained by the influence of the Fe environment on the hyperfine interactions. Since $Y(Fe_xAl_{1-x})_2$ crystallizes in the cubic $MgCu_2$ structure (C15), with the exception of a small concentration region around $x = 0.50$, where the hexagonal $MgZn_2$ (C14) structure is stable, the Fe and Al atoms, which occupy the 16d sites, are surrounded by six nearest Fe or Al neighbours and six Y neighbours. Therefore six different Fe environments are possible if only nearest-neighbour interactions are taken into account.

The ^{57}Fe transmission Mössbauer spectra taken in applied fields are magnetically split (figure 1). These spectra can be analysed assuming that the hyperfine parameters are mainly influenced by the number of nearest Fe neighbours surrounding the ^{57}Fe nucleus. Since Fe and Al atoms are randomly distributed over the 16d positions according to x-ray investigations, the number and the intensity ratios of the subspectra are given by the binomial distribution function, which leads to the following: five subspectra (Fe surrounded by zero to four nearest Fe neighbours) with relative intensities of 0.178, 0.356, 0.297, 0.132 and 0.033 for $x = 0.25$; six subspectra (zero to five nearest Fe neighbours) with 0.047, 0.187, 0.311, 0.277, 0.138 and 0.037 for $x = 0.40$; six subspectra (one to six nearest Fe neighbours) with relative intensities 0.021, 0.095, 0.236, 0.328, 0.244 and 0.075 for the

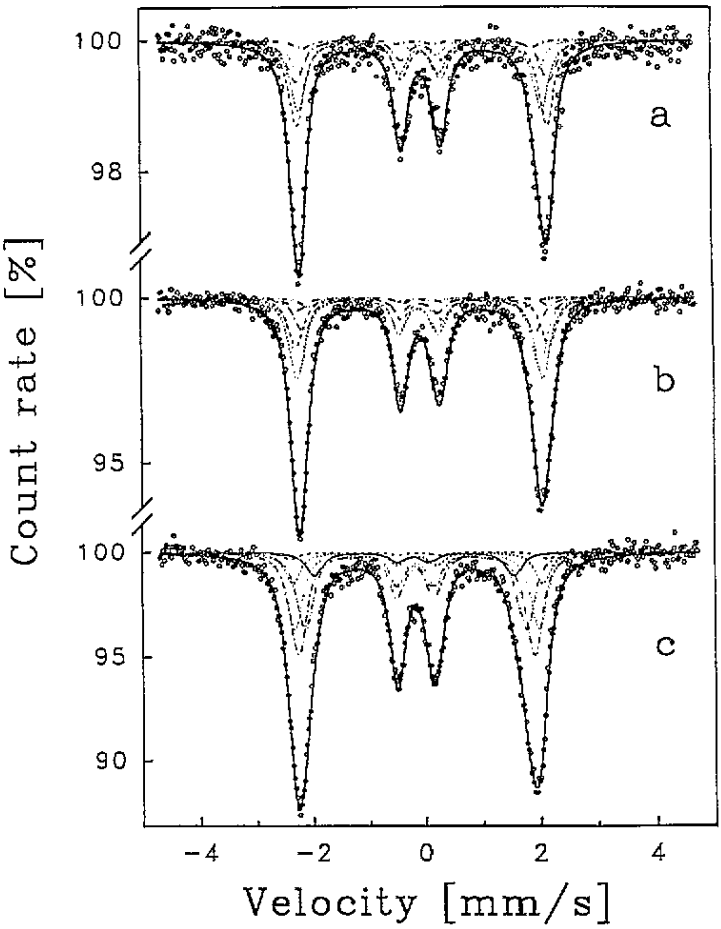

Figure 1. ^{57}Fe transmission Mössbauer spectra of $Y(Fe_xAl_{1-x})_2$ at room temperature and $B_a = 13.5$ T for (*a*) $x = 0.25$, (*b*) $x = 0.40$ and (*c*) $x = 0.65$: ○, measured points; ——, calculated spectra. The calculated subspectra for the different Fe environments are also shown — — — only Al nearest neighbours; – – –, one nearest Fe neighbour; ----, two nearest Fe neighbours; ·····, three nearest Fe neighbours; — · —, four nearest Fe neighbours; — · · —, five nearest Fe neighbours; ——, six nearest Fe neighbours.

sample with $x = 0.65$; five subspectra (two to six nearest Fe neighbours) with intensities 0.033, 0.132, 0.297, 0.356 and 0.178 for $x = 0.75$.

The shape of the spectra shows clearly that the effective magnetic hyperfine fields are aligned parallel to the external field B_a, since the second and fifth lines ($\Delta m = 0$) are not present in the spectra (figure 1) and B_{hf} is always smaller than B_a (where B_{hf} is the field acting on the ^{57}Fe nucleus). The absorption lines on the low-energy side of the spectrum are narrower and deeper. This asymmetry of the spectra is caused by the different centre shifts and effective fields for the various Fe environments.

The resulting induced hyperfine field B_{ind} is deduced from the recorded spectra by

$$B_{ind} = B_a - B_{hf} \tag{2}$$

and increases with increasing number of Fe neighbours (figure 2). A Curie–Weiss law

$$B_{ind}/B_a = C_{ind}^{MB}/(T-\theta) \tag{3}$$

can be fitted to the data of each subspectrum using the θ-values determined by magnetization measurements from [5], leading to a Curie constant C_{ind}^{MB} derived by Mössbauer effect measurements. (The uncertainties in the Mössbauer data make it impossible to derive θ directly from the fit.) The values used for θ are 0 K, 0 K, 20 K and 173 K for $x = 0.25$, 0.40, 0.65 and 0.75, respectively. C_{ind}^{MB} increases with increasing number of nearest Fe neighbours for each Fe concentration (figure 3). Therefore the mean value, given by the large full diamonds in figure 3, increases with increasing Fe concentration. The slight decrease in C_{ind}^{MB} for a fixed Fe environment with increasing x will be shown below to be associated with the decrease in lattice constant.

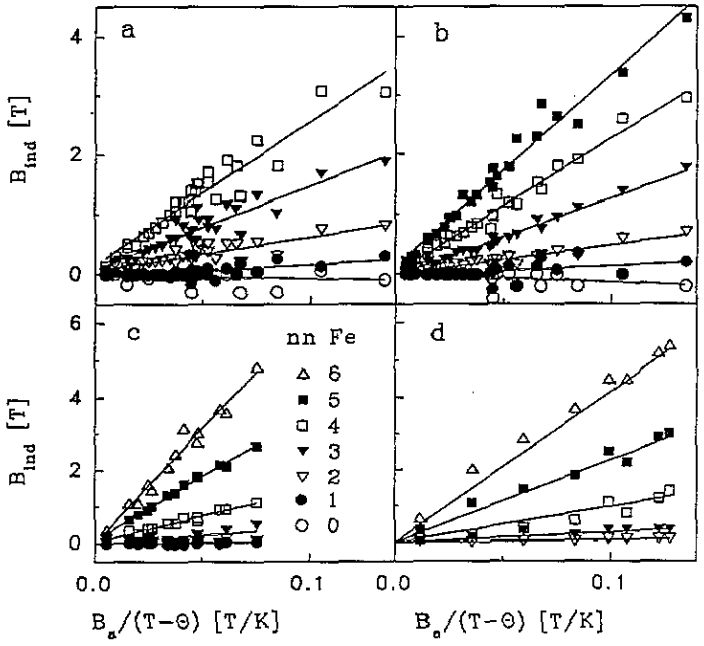

Figure 2. Dependence of the induced hyperfine fields in $Y(Fe_xAl_{1-x})_2$ on $B_a/(T-\theta)$ for (*a*) $x = 0.25$, (*b*) $x = 0.40$, (*c*) $x = 0.65$ and (*d*) $x = 0.75$: the symbols represent the different numbers of nearest Fe neighbours (nn Fe) as shown; ——, linear regressions to the data.

The present LAPW band-structure calculations for YFe_2, Y_2Fe_3Al and Y_2FeAl_3 yield Fe moments of $1.98\mu_B$, $1.57\mu_B$ and $1.93\mu_B$, respectively. The Y moment is antiparallel and large in YFe_2 ($-0.42\mu_B$) but decreases with Al substitution to smaller values ($-0.31\mu_B$ and $-0.08\mu_B$). These results show that effective iron moments can be deduced from magnetization measurements on the Al-rich side, but the effective iron moments would be underestimated on the Fe-rich side owing to partial cancellation between the antiparallel Fe and Y moments. Hyperfine fields B_{tot}^{th} are computed by means of LAPW and ASW band-structure calculations for these ordered structures (plus $Y_2Fe_2Al_2$ with ASW only). Two contributions to hyperfine field B_{tot}^{th} are found: an almost x-independent contribution B_{core}^{th} from the core and a contribution B_{val}^{th} with opposite sign originating from the valence electrons (4s and 4p). The latter (B_{val}^{th}) decreases approximately linearly with increasing Fe concentration (figure 4).

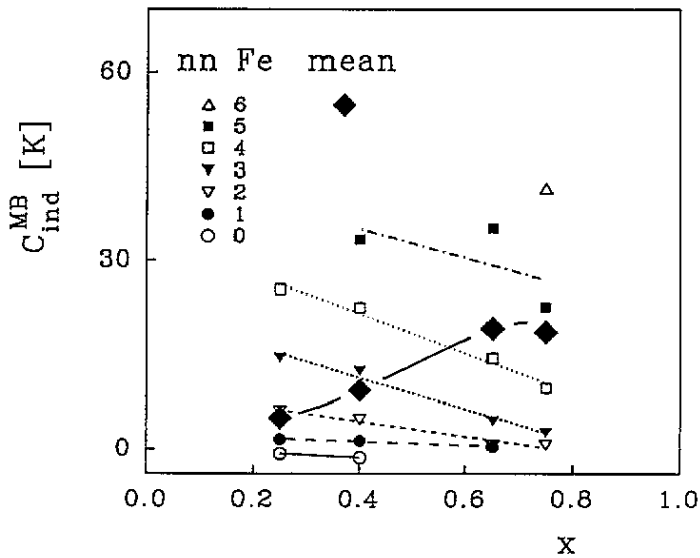

Figure 3. Dependence of C_{ind}^{MB} (defined by equation (3)) on the Fe concentration for the different environments, i.e. number of nearest Fe neighbours (nn Fe) (and mean value): lines are guides to the eyes.

The core hyperfine field B_{core}^{th} is negative and proportional to the respective Fe 3d moment. For YFe_2, B_{val}^{th} is very small, so that the total hyperfine field arises almost entirely from the core polarization and thus is proportional to the Fe moment, the usual assumption made for interpreting Mössbauer measurements [21]. With increasing Al concentration, however, B_{val}^{th} increases strongly owing to a strong positive polarization of the valence Fe 4s (and 4p) electrons which nearly (for high Al concentrations) compensates the large negative B_{core}^{th}. Such a positive polarization of the 4s electrons (i.e. parallel to the 3d moment) is quite unusual, since for most systems studied so far the 4s polarization is small and negative. For instance, Eriksson and Svane [27] found only two systems, namely the insulators FeO and Fe_2P, which exhibit a large Fe valence contribution to B_{tot}^{th}. They argue that in these compounds the majority Fe d band is fully occupied and thus the direct parallel 4s mixing dominates the usual antiparallel 4s–3d hybridization. However, energy band calculations based on the LSDA are known to have difficulties (and sometimes fail) in describing systems with localized moments or insulating antiferromagnets. Therefore, it is not too surprising that the calculated hyperfine fields differ considerably from experiment for these two compounds. Although Y_2FeAl_3 is metallic, it still shows this unusual behaviour of the 4s electrons.

In order to investigate the volume dependence of the hyperfine field, additional calculations with different lattice constants were carried out, keeping the respective composition fixed. For example, one reduces the lattice constant of Y_2Fe_3Al (corresponding to $x = 0.75$) from its equilibrium value of 7.48 Å to 7.36 Å, the corresponding value for YFe_2, so that one can associate this volume change with a variation in x from 0.75 to 1.0. The volume dependence of the different B^{th} contributions can then be displayed as a function of x (full lines in figure 4). The resulting slopes are nearly the same for all compositions and differ significantly from the concentration dependence, so that changes in volume cannot account for the observed x dependence of the hyperfine fields. This result is in contrast with the isomer shifts, where the change in volume is responsible for at least half

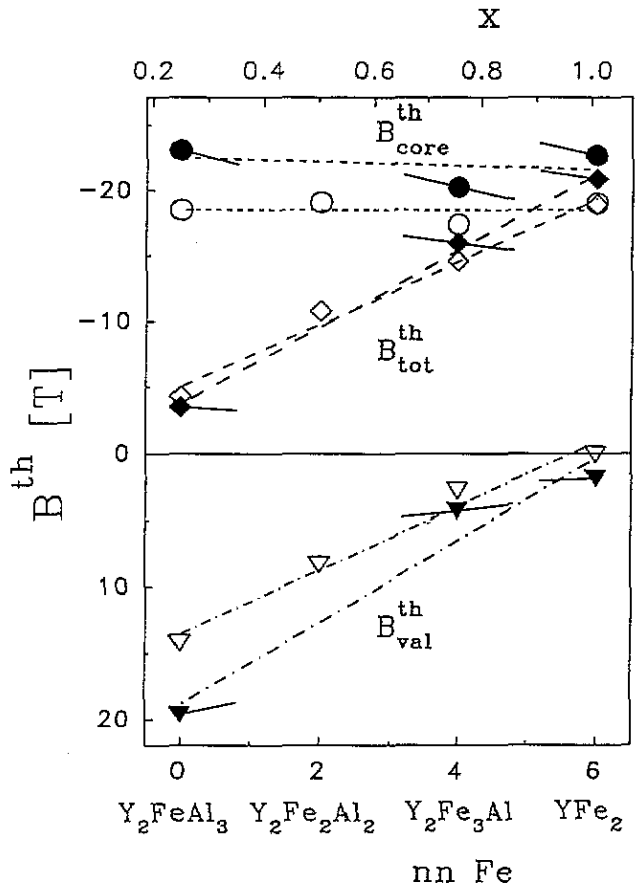

Figure 4. Calculated (○, ◇, ▽, ASW; ●, ◆, ▼, LAPW) hyperfine fields in $Y(Fe_xAl_{1-x})_2$: ○, ●, B^{th}_{core}; ◇, ◆, B^{th}_{tot}; ▽, ▼, B^{th}_{val}; — — —, — · —, guides to the eyes; ——, corresponding volume dependence, where the linear variation in the lattice constants was used to convert volume to composition.

the concentration dependence [33]. However, the negative slope of the volume dependence of B^{th}_{tot} corresponds to the experimentally observed decrease in C^{MB}_{ind} for a fixed number of nearest Fe neighbours (figure 3).

The ratio of the number of Fe to Al atoms defines the Fe concentration x (upper horizontal scale in figure 4). Since the calculations were done for ordered structures, in which each Fe atom is surrounded by a fixed number of Al atoms, the number of nearest neighbours (given on the scale at the bottom of figure 4) can be correlated with x, allowing one to compare theoretical results with experimental data at the same concentration. However, one should keep in mind that the calculations are carried out with the experimentally observed lattice constant and that they correspond at best to only one Fe environment used in the analysis of the Mössbauer spectra. Owing to the large difference between the atomic radii of Fe and Al, the interatomic distances vary locally for the different environments. These internal modulations lead to differences in the local lattice spacing and cause a broadening of the peaks in the x-ray diffraction patterns. The latter can be converted to a change in Fe concentration of about 3 at.% [35] as judged by the measured

variation in the average lattice constant with Fe content.

Nevertheless the dependence of B_{tot}^{th} on the number of nearest Fe neighbours as well as on the concentration shows the same trend as the experimental quantity C_{ind}^{MB} (figure 5).

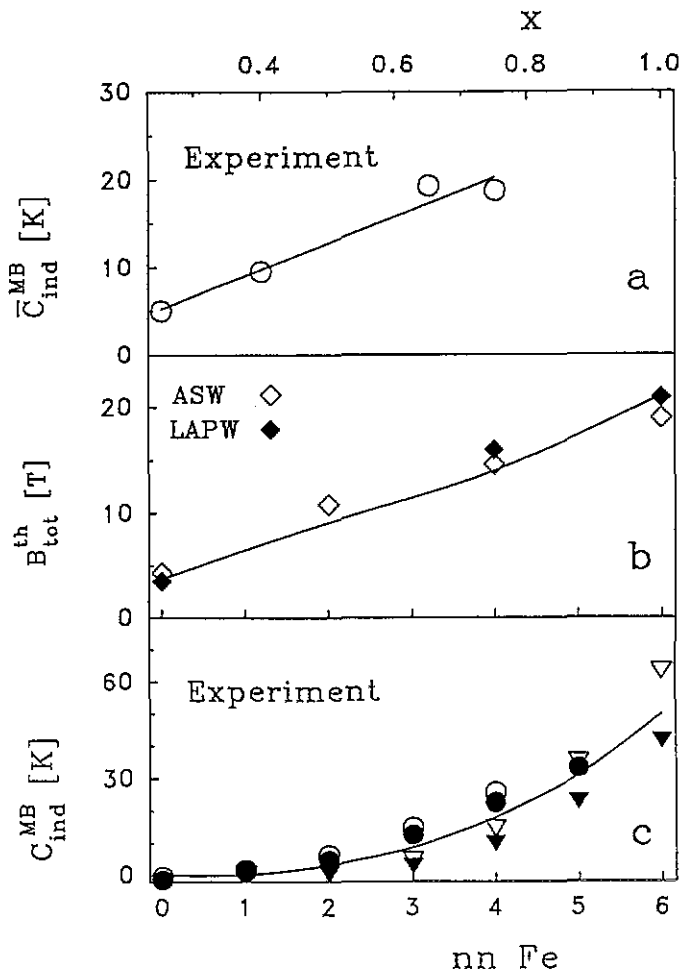

Figure 5. Comparison of theoretical and experimental hyperfine fields and their dependence on x and number of nearest Fe neighbours (nn Fe) (——, guides to the eyes): (*a*) dependence of $\bar{C}_{ind}^{MB}$ (derived from Mössbauer spectroscopy) on x; (*b*) dependence of B_{tot}^{th} on x and nn Fe as obtained from ASW (◇) and LAPW (◆) band-structure calculations for ordered (only one distinct environment) Y_2FeAl_3, $Y_2Fe_2Al_2$, Y_2Fe_3Al and YFe_2 compounds; (*c*) dependence of C_{ind}^{MB} on nn Fe for different Fe concentrations (○, $x = 0.25$; ●, $x = 0.40$; ▽, $x = 0.65$; ▼, $x = 0.75$).

5. Discussion

In order to determine the local susceptibility χ_{loc} it is necessary to relate the measured induced hyperfine field to the magnetic moment. Commonly a direct proportionality between

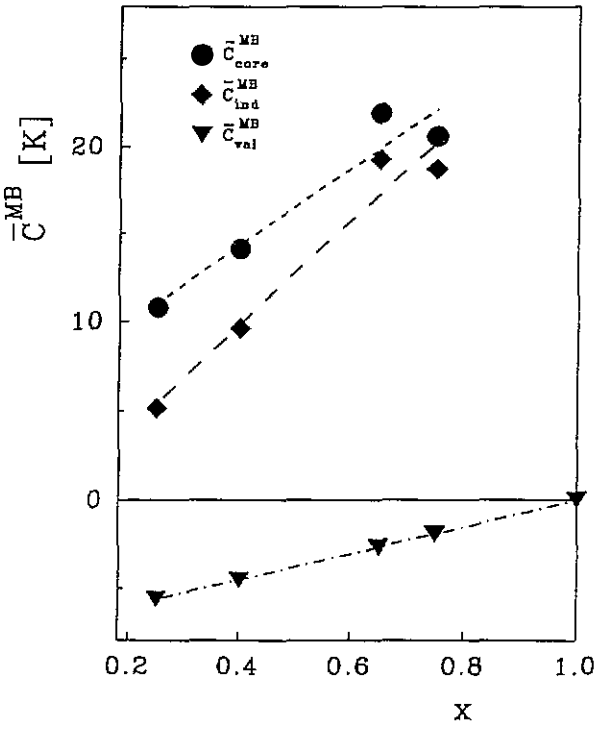

Figure 6. Dependence of the mean values of $\bar{C}^{MB}_{ind}$, the core contribution $\bar{C}^{MB}_{core}$ and the valence contribution $\bar{C}^{MB}_{val}$ on the Fe concentration x.

B_{hf} and the Fe moment is assumed. It was shown that this simple *ansatz* can explain the measured fields in many systems, e.g. Fe–B alloys [21].

Using the same procedure leads to local susceptibilities for Y(Fe,Al)$_2$ which vary for the different environments. Summing these susceptibilities and weighting them with the appropriate probabilities for their appearance (given by the ratio of the corresponding binomial distributions) give a mean susceptibility that increases with increasing Fe content in agreement with bulk magnetic measurements [11], but with a different slope. This deviation in slope can arise if either the hyperfine coupling constants are different for the various samples, or this *ansatz* is too simple. Even if the direct proportionality between B_{ind} and μ_{Fe} is correct, the problem concerning the Fe moments remains, since bulk magnetic measurements point to a stable Fe moment in the whole concentration range while B_{ind} decreases strongly with decreasing number of nearest Fe neighbours, so that B_{ind} is close to zero when Fe is surrounded by only Al (figure 2).

It has been shown that for 3d impurities in ferromagnetic rare-earth hosts the hyperfine field is determined not only by polarization of the core electrons but also by a large contribution from polarization of the conduction electrons [36]. The same type of results is obtained from the band-structure calculations for Y(Fe,Al)$_2$ (figure 4). Therefore, it is necessary to decompose the values of B_{ind} into a contribution B_{core} from the core electrons and a B_{val} contribution originating from the valence electrons. The local susceptibility related to B_{core} can now be compared with the local Fe moment, because both originate from the d electrons. Since both B_{ind}/B_a (equation (3)) and the susceptibility χ^{mag} determined

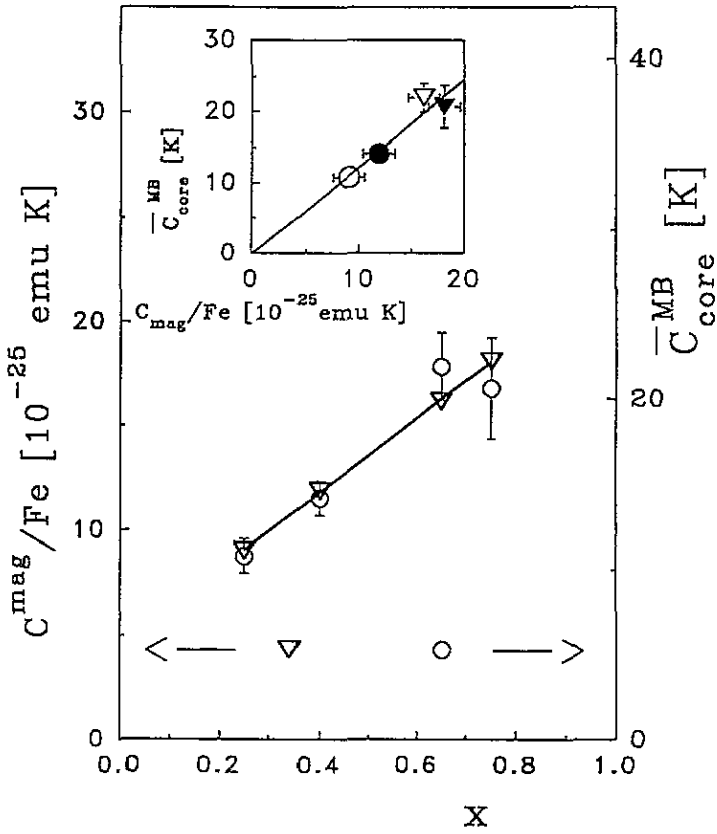

Figure 7. Comparison of the x dependence of C^{mag} per Fe atom from magnetization measurements (▽, left-hand scale) with that of $\bar{C}^{MB}_{core}$ from Mössbauer measurements (○, right-hand scale). The inset shows $\bar{C}^{MB}_{core}$ as a function of C^{mag} for different concentrations: ○, $x = 0.25$; ●, $x = 0.40$; ▽, $x = 0.65$; ▼, $x = 0.75$; ——, linear regression to the data.

from bulk magnetic measurements follow a Curie–Weiss law, a dependence of B_{core}/B_a according to $C^{MB}_{core}/(T-\theta)$ was assumed. With this assumption, B_{val}/B_a must also follow a Curie–Weiss law.

For the partition of B_{ind} into B_{core} and B_{val} the results of the band-structure calculations were used. Since according to the calculations the valence contribution to the hyperfine field decreases approximately linearly with increasing x and is close to zero for YFe_2 (figure 4), a similar concentration dependence was assumed for $\bar{C}^{MB}_{val}$, leaving only the slope as the free parameter. This slope can be estimated by assuming direct proportionality between the mean (concerning the different environments for one concentration) of the core contribution $\bar{C}^{MB}_{core}$ and the magnetically determined Curie constant C^{mag}. The result of such a partition is given in figure 6. In order to allow for a comparison of the extensive variable C^{mag} with the intensive variable $\bar{C}^{MB}_{core}$ the former was related to a single Fe atom. The comparison demonstrates that both variables increased linearly with increasing x (figure 7), indicating that the assumed direct proportionality of $\bar{C}^{MB}_{core}$ to C^{mag} (inset of figure 7) is consistent with the data. Therefore, it can be concluded that there is only one hyperfine coupling constant between the induced hyperfine field and the magnetic moment for the whole concentration range. The concentration dependence of the core contribution of the induced hyperfine

field, which is determined from the Mössbauer investigations, is in excellent agreement with the concentration dependence of the effective Fe moment determined from bulk magnetic measurements.

The values of C_{val}^{MB} and C_{core}^{MB} for the individual environments can be derived from the respective mean values and the measured B_{ind} for the different surroundings, if one assumes that C_{val}^{MB} decreases linearly with increasing number of nearest Fe neighbours. This assumption has already been made for the dependence of the average value $\bar{C}_{val}^{MB}$ on x. Now the components to C_{core}^{MB} and the corresponding local susceptibilities are determined from $\chi_{loc} = B_{core}/B_a$ with $B_{core} = C_{core}^{MB} B_a/(T-\theta)$. For up to three nearest Fe neighbours C_{core}^{MB} remains nearly constant but it increases for more nearest Fe neighbours (figure 8). This result indicates that Fe carries a moment even if surrounded by only aluminium, a fact in good agreement with the results of the band-structure calculations (figure 4). The increase in C_{core}^{MB} with increasing number of nearest Fe neighbours for the Fe-rich cases reflects the concentration dependence of $\bar{C}_{core}^{MB}$ and μ_{eff}.

However, the theoretical values for the core contribution B_{core}^{th} stay more or less constant. As mentioned above, one should not compare these theoretical results with the experimental data in too much detail, since the calculations are performed for ordered structures, in which only one distinct Fe surrounding is present and ferromagnetic spin alignment was assumed.

The present results strongly indicate that both the valence and the core contributions to the measured hyperfine field must be taken into account, in order to estimate the Fe moment from these data.

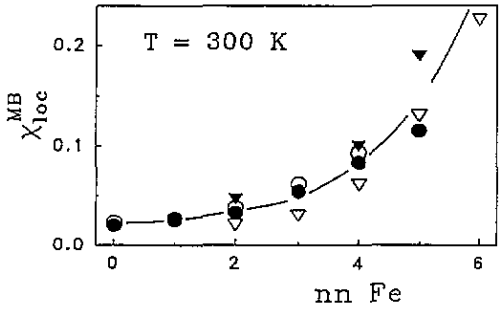

Figure 8. Dependence of the local susceptibility χ_{loc} on the number of nearest Fe neighbours (nn Fe) in $Y(Fe_xAl_{1-x})_2$ at 300 K: ○, $x = 0.25$; ●, $x = 0.40$; ▽, $x = 0.65$; ▼, $x = 0.75$; ——, guide to the eyes.

6. Conclusion

The induced hyperfine fields for Fe surrounded by only Al, and for Fe with one Fe and five Al neighbours are very low compared with those where Fe has more than one Fe nearest neighbour.

An interpretation that B_{ind} originates from only the Fe moments is in contradiction to the fact that μ_{eff} per Fe atom is close to $2\mu_B$ for $x = 0.1$. Furthermore, ASW and LAPW calculations of ordered Y_2FeAl_3, $Y_2Fe_2Al_2$ and Y_2Fe_3Al and of YFe_2 at $T = 0$ lead to two contributions (with different signs) to the hyperfine field B_{tot}^{th}, which have almost the same magnitude at low Fe concentrations. This indicates the importance of the valence electrons for the hyperfine fields in these systems.

The subdivision of B_{ind} into two parts, namely a core contribution B_{core} and a valence contribution B_{val}, where the lattice increases linearly with increasing x and is opposite in

sign to B_{core}, leads to similar dependences of $\bar{B}_{ind}$, $\bar{B}_{core}$ and $\bar{B}_{val}$ on x as for the theoretical values B^{th}_{tot}, B^{th}_{core} and B^{th}_{val}. The values of $\bar{B}_{core}$ are proportional to the magnetically determined Curie constants independent of x. The local susceptibilities are nearly constant for environments with up to three nearest Fe neighbours and increase for more than three nearest Fe neighbours.

Acknowledgment

This work was supported in part by the Austrian Science Foundation (FWF) project No P6938.

References

[1] Buschow K H J 1975 *J. Less-Common Met.* **40** 361
[2] Besnus M J, Bauer P and Genin J M 1978 *J. Phys. F: Met. Phys.* **8** 191
[3] Steiner W 1979 *J. Magn. Magn. Mater.* **14** 47
[4] Hilscher G, Grössinger R, Sechovsky V and Nozar P 1982 *J. Phys. F: Met. Phys.* **12** 1209
[5] Reissner M, Steiner W, Kappler J P, Bauer P and Besnus M J 1984 *J. Phys. F: Met. Phys.* **14** 1249
[6] Reissner M and Steiner W 1986 *Hyperfine Interact.* **28** 1017
[7] Nozar P, Sechovsky V and Kambersky V 1987 *J. Magn. Magn. Mater.* **69** 71
[8] Steiner W, Reissner M, Moser J and Will G 1988 *Physica* B **149** 329
[9] Cunha S F da, Souza G P and Takeuchi A Y 1988 *J. Magn. Magn. Mater.* **73** 355
[10] Kasprzyk A, Zarek W and Slebarski A J 1989 *J. Less-Common Met.* **147** 121
[11] Pösinger A, Reissner M and Steiner W 1989 *Physica* B **155** 211
[12] Pösinger A, Winkler H, Steiner W, Trautwein A X and Reissner M 1991 *J. Phys.: Condens. Matter* **3** 2713
[13] Yamada H, Inoue J, Terao K, Kanada S and Shimizu M 1984 *J. Phys. F: Met. Phys.* **14** 1943
[14] Mohn P and Schwarz K 1985 *Physica* B **130** 26
[15] Ritter C 1989 *J. Phys.: Condens. Matter* **1** 2765
[16] Steiner W, Haferl R and Grössinger R 1980 *J. Physique* **41** C1 193
[17] Steiner P, Beloserskij G N, Gumprecht D, Zdrojewski W v and Hüfner S 1973 *Solid State Commun.* **13** 1507
[18] Scherg M, Seidel E R, Litterst F J, Gierisch W and Kalvius G M 1974 *J. Physique* **35** C6 527
[19] Campbell S J, Clark P E and Hicks T J 1977 *Solid State Commun.* **24** 791
[20] Chappert J, Teillet J and Varret F 1979 *J. Magn. Magn. Mater.* **11** 200
[21] Vincze I, Balogh J, Foris Z, Kaptas D and Kemeny T 1991 *Solid State Commun.* **77** 757
[22] Aoki M and Yamada H 1989 *J. Magn. Magn. Mater.* **78** 377
[23] Aoki M and Yamada H 1989 *Solid State Commun.* **72** 21
[24] Rizzuto C 1974 *Rep. Prog. Phys.* **37** 147
[25] Grüner G 1974 *Adv. Phys.* **23** 941
[26] Deuz J, Dederichs P H and Zeller R 1981 *J. Phys. F: Met. Phys.* **11** 1787
[27] Eriksson O and Svane A 1989 *J. Phys.: Condens. Matter* **1** 1589
[28] Guenzburger D and Ellis D E 1992 *J. Magn. Magn. Mater.* **104–7** 2009
[29] Gabriel J R and Ruby S L 1965 *Nucl. Instrum. Methods* **36** 23
[30] Mørup S and Both E 1975 *Nucl. Instrum. Methods* **124** 445
[31] Williams A R, Kübler J and Gelatt C D Jr 1979 *Phys. Rev.* B **19** 6094
[32] Blaha P, Schwarz K, Sorantin P and Trickey S B 1990 *Comput. Phys. Commun.* **59** 399
[33] Blaha P, Schwarz K and Ray A K 1992 *J. Magn. Magn. Mater.* **104–7** 683
[34] Blügel S, Akai H, Zeller R and Dederichs P H 1987 *Phys. Rev.* B **35** 3271
[35] Reissner M 1990 *Thesis* Technische Universität Wien
[36] Leal C E and Troper A 1990 *J. Appl. Phys.* **67** 5876